THE JOURNAL OF PHYSICAL CHEMISTRY B

ARTICLE

pubs.acs.org/JPCB

Effect of Counterions on the Protonation State in a Poly(G)−Poly(C) Radical Cation

Jian Wu, Laura Albrecht, and Russell J. Boyd*

Department of Chemistry, Dalhousie University, Halifax, Nova Scotia, Canada B3H 4R2

ABSTRACT: The proton transfer process from a guanine to its complementary cytosine in a B-form d[GG] radical cation is investigated theoretically. The d[GG] radical cation is optimized by the ONIOM + PCM method. In this two-layer ONIOM method, the high layer consists of the π-stacked complementary base pairs with a hole charge, which is treated at the B97D/6-31G(d) level. The low layer includes the sugar−phosphate backbone and sodium ions, which is treated with the Amber99SB/Parmbsc0 force field. Our calculations reveal that the stabilization of the deprotonated state in d[GG] oligomers is related to the location of sodium ions. When sodium ions are located near phosphate groups, the proton prefers bonding with the guanine, and 80% of the hole charge is delocalized on the guanine residues. When sodium ions are placed in the major groove, the deprotonated state is favorable, and 70% of the hole charge localizes on the corresponding guanine−cytosine pair. According to the natural bond orbital analysis, the N−H···N hydrogen bond between the guanine−cytosine pair provides an important contribution to the stabilization of the deprotonated state. Stabilization of this hydrogen bond is very sensitive to the d[GG] oligomer configuration. In summary, the proton transfer process in a guanine−cytosine pair of poly(G)−poly(C) radical cations is largely affected by the arrangement of counterions.

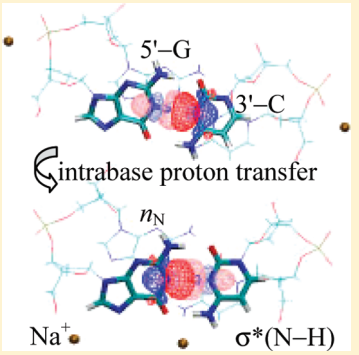

I. INTRODUCTION

As one characteristic of DNA oxidative damage, the oxidative reaction is usually detected at guanine base sites with two or three adjacent guanines (G_n (n = 2−3)).[1−3] The oxidation reaction occurs primarily at guanines because they have low oxidation potentials[4−6] and can trap the radical cation from a remote site via DNA-mediated electron transfer.[7,8] Theoretical investigations of charge distribution on guanine bases in DNA radical cations focus typically on two aspects: whether the hole charge in DNA is confined to a single base pair or delocalized over several bases and whether there exists intrabase proton transfer between guanine and its complementary cytosine. Ab initio[9−14] and model Hamiltonian[15−20] calculations have shown that the hole charge delocalizes over three guanine bases. However, theoretical calculations also reveal that solvent and counterions surrounding DNA affect the charge distribution on the guanine bases and even lead to charge localization.[21−23]

Recently, the extent of hole delocalization in G-stacked systems was studied using the M06-2X/6-31G* method. The optimized geometries of G-stacked (GG and GGG) radical cations in the B-DNA conformation showed that the hole charge is predominantly localized on a single guanine.[24] However, in this calculation, the sugar−phosphate backbone of DNA, counterions, and solvation were not included. Furthermore, two dihedral angles ($N_{7a}N_{7b}N_{9b}N_{9a}$ and $N_{3a}N_{3b}C_{6b}C_{6a}$) and four angles ($N_{7a}N_{7b}N_{9b}$, $N_{7b}N_{9b}N_{9a}$, $N_{3a}N_{3b}C_{6b}$, and $N_{3b}C_{6b}C_{6a}$) between two adjacent bases, a and b as shown in Figure 1, were constrained artificially to keep the DNA conformation in the B-form. Without the backbone restraint, geometry optimization of the π stacks would result in loss of the B-DNA conformation.

The second discussion concerns a proton transfer from the N_1 of a guanine (N_1(G)) to the N_3 of the complementary cytosine (N_3(C)). A guanine−cytosine (G−C) pair and its atom numbers are shown in Figure 1, where C′ and C″ represent G−C pairs bonded to sugars in DNA. The intrabase proton transfer in a G−C cation is a prototropic equilibrium process[25] between a $G^{\bullet+}$:C radical cation and a deprotonated G(−H)·:C(+H)$^+$ base pair. With the deprotonation process in a G−C cation, the positive charge is being stabilized on the single G−C base pair. Experiments have shown the important contribution of the intrabase proton to the charge transfer in DNA.[26,27] Furthermore, a complete proton transfer in a G−C cation has been observed at 77 K in DNA oligomers.[28] First principles molecular dynamics calculations on Z-DNA oligomers revealed that the deprotonated state localizes the hole charge.[12] However, most calculations on the deprotonated state have been performed on the radical cation with a single G−C pair.[29−33] To consider the solvent effect, the geometry of a G−C radical cation with 11 water molecules was also optimized.[32]

In this paper, the properties of the cationic d[GG] oligomer with the deprotonated state are investigated. It is known that the electronic properties of DNA are very sensitive to the DNA conformation.[13,34−36] Furthermore, they are also strongly affected by solvent and counterions.[11,21,23,37−40] For example, quantum mechanics−molecular mechanics (QM/MM) calculations show that the fluctuations of nucleobase onsite energies

Received: September 26, 2011
Revised: October 24, 2011
Published: October 26, 2011

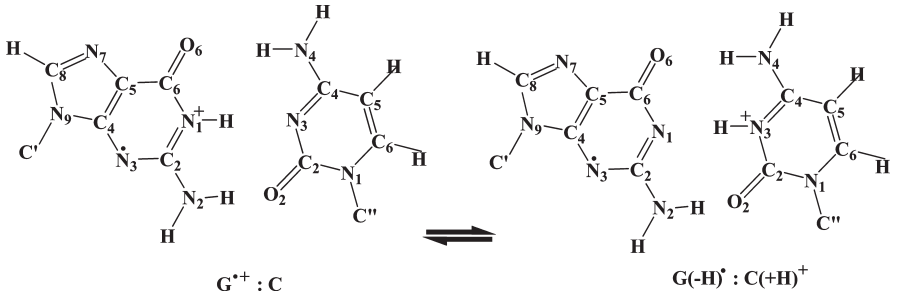

Figure 1. The intrabase proton transfer in a G−C base pair between a G•+:C radical cation and a deprotonated G(−H)•:C(+H)+ base pair.

induced by solvent are ~0.4 eV, of which only 0.1 eV is a result of the internal motion of bases.[23] Voityuk's model calculations[37] suggest that the hole in 5′-XGGY-3′ duplexes is localized due to the effects of solvation and DNA structural reorganization. DFT calculations on the electronic density of states reveal that sodium ions (Na^+) take part in the charge transfer in DNA.[40] Therefore, a geometry optimization of the DNA molecule is necessary to describe the deprotonated state and charge distribution in d[GG] oligomers. Counterions and solvation cannot be neglected. Our previous work[14] has shown that the two-layer ONIOM method[41,42] provides a reliable and feasible model to perform this calculation. The detailed computational model for d[GG] oligomer is described in section II. The results of the calculations are discussed in section III.

II. COMPUTATION MODELS

A standard d[GG] oligomer was generated by means of the Nucleic Acid Builder (NAB).[43] In this initial geometry of the DNA radical cation, the intrabase proton is bonded to the N_1 atom of the 5′-end guanine. The initial deprotonated geometry was generated by shifting the intrabase proton from the N_1 atom of the 5′-end guanine (N_1(G)) to the N_3 atom of its paired cytosine (N_3(C)). The counterion selected is the sodium ion (Na^+). The two sodium ions were placed at different locations to investigate the effect of counterions. The locations of sodium ions were arranged according to the LEaP program embedded in AmberTools.[44] In the first arrangement, each Na^+ is located near a different phosphate group. The second arrangement places both sodium ions in the major groove, one near atom N_7 of the 3′-end guanine; the other, close to the 5′-end guanine. The first locations of the sodium ions have lower electrostatic potentials (ESP) than the second locations. Hence, there are four different geometries (**1**, **1d**, **2**, **2d**) of d[GG] oligomer to be investigated. The corresponding proton positions and Na^+ arrangements of these four geometries are listed in Table 1, and their geometries are plotted in Figure 2.

These four initial geometries were optimized by use of a two-layer ONIOM method.[14] In this ONIOM calculation, the system is divided into two regions, which are referred to as the high layer and the low layer. The high layer consists of the π-stacked complementary base pairs. This layer mediates the charge transfer in DNA,[45] and its geometry is our primary interest. Inclusion of dispersion is very important in the high layer to correctly describe the π-stacking interactions of nucleobases and the hydrogen bonds between complementary base pairs.[46−49] Calculations on aromatic hydrocarbons indicate that the B97D functional predicts geometries in good agreement with experiment.[48] In our calculation the high layer was treated at the B97D/6-31G(d) level. The low layer includes the sugar−phosphate backbone and sodium ions and was treated with the Amber99SB force field, including the parmbsc0 correction with improved parameters on the DNA backbone.[50−52] Solvent effects were included by using the polarizable continuum model (PCM).[53] The natural bond orbital (NBO) analysis[54] was employed to study the charge distributions and hydrogen bonds between bases pairs. All calculations were performed with the Gaussian 09 package.[55] The VMD[56] software package was used for graphical representations of results.

Table 1. Characteristics of Four Initial Geometries for d[GG] Oligomer

	1	1d	2	2d
protonation state	protonated	deprotonated	protonated	deprotonated
ESP values of Na^+	low	low	high	high

III. RESULTS AND DISCUSSION

(A). Efficiency of the ONIOM + PCM Method. The initial geometry generated by NAB comes from experimental B-form DNA parameters. This geometry is used as a standard to evaluate the performance of the ONIOM + PCM method through comparison with the optimized geometries of oligomers **1** and **2**. Figure 3 plots the superposition of the standard d[GG] geometry with the optimized geometries of oligomers **1** and **2**. The standard geometry is plotted using a tube frame in which all atoms are colored according to their atom types. The optimized geometry of **1** corresponds to the red wireframe. The optimized geometry of **2** is green. Neglecting all hydrogen atoms, root-mean-square deviation (rmsd) values between the standard geometry and the two optimized geometries are 0.916 and 0.876 Å for **1** and **2**, respectively. These results are comparable to the previous ONIOM method,[14] in which solvent effects were considered by adding an 8.0 Å water box around the DNA oligomer. Therefore, the ONIOM + PCM model is acceptable for the geometry optimization of the DNA model systems.

(B). Stabilization of the Deprotonation State. When sodium ions are at the low ESP positions, the optimized **1** geometry is 1.92 kcal/mol more stable than the optimized **1d** geometry. However, when sodium ions are placed at the high ESP positions, the optimized **2d** geometry is 0.71 kcal/mol more stable than the optimized **2** geometry. In other words, the deprotonated state is affected by the counterion location. Our stabilization energy is comparable to the B3LYP[32] and MP2[33] results obtained for a single G−C radical cation. The stabilization energies at the B3LYP and MP2 levels are 1.2 and 1.7 kcal/mol, respectively. The stabilization energy of the deprotonated state at the B3LYP

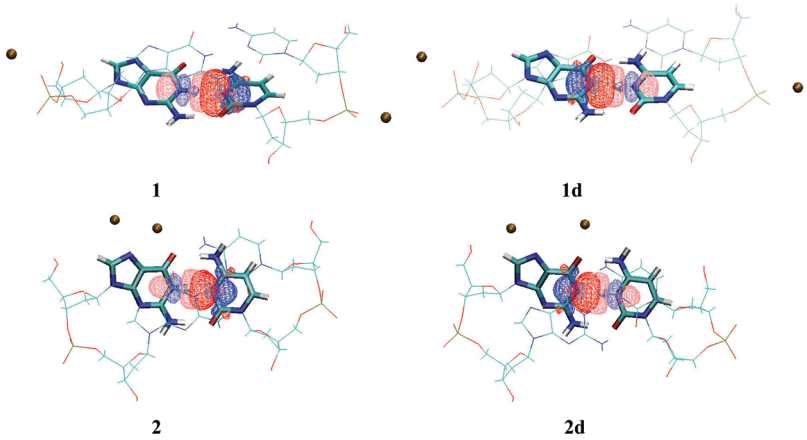

Figure 2. Four ONIOM systems of d[GG] oligomers with sodium ions and NBO images of the N−H···N hydrogen bond between the G_1−C_1 base pair. G_1−C_1 base pairs are plotted in the tube format to distinguish them from the G_2−C_2 base pairs. Positive and negative isosurfaces of the NBOs at an isovalue of 0.02 are represented as red and blue surfaces, respectively. Dark surfaces represent donor orbitals and light surfaces represent acceptor orbitals. For oligomers **1** and **2**, the donor orbital is the lone pair orbital $n(N_3(C_1))$, and the acceptor orbital is the antibonding orbital $\sigma^*(N_1(G_1)\cdots H)$. For oligomers **1d** and **2d**, the donor orbital is the lone pair orbital $n(N_1(G_1))$, and the acceptor orbital is the antibonding orbital $\sigma^*(H\cdots N_3(C_1))$.

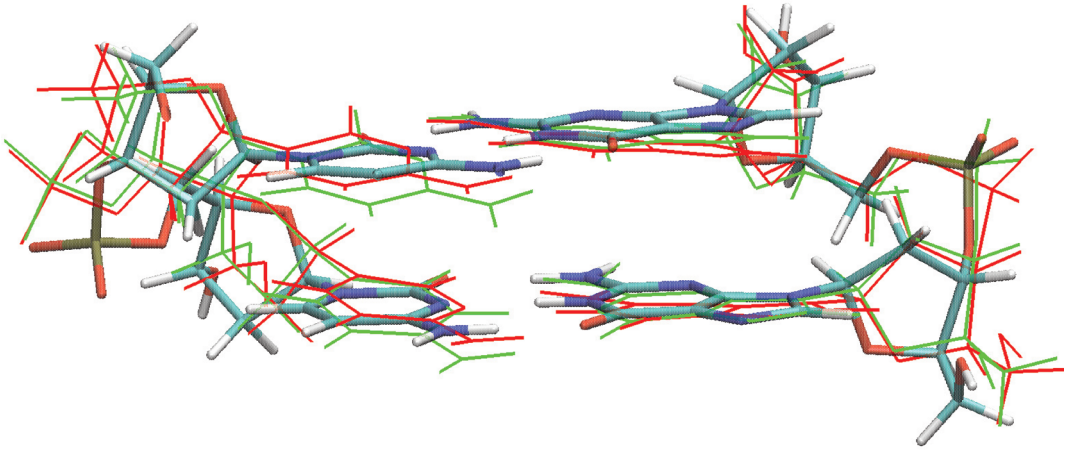

Figure 3. Superposition of the standard d[GG] geometry and the optimized geometries of oligomers **1** and **2**. The standard geometry is plotted by a tube frame in which all atoms are colored according to their atom types. The optimized geometry of **1** is the red wireframe, and **2** is green.

level, which neglects the dispersion interaction within base pairs, is 0.5 kcal/mol higher than the stabilization energy at the MP2 level. Our stabilization energy for the d[GG] oligomer is 1.00 kcal/mol smaller than the MP2 calculation for one G−C pair.[33] To reveal the effects of π-stacking and the sugar−phosphate backbone, the energies of one and two G−C base pairs, which have been extracted from the optimized **1**, **1d**, **2**, and **2d** oligomers were calculated. Here, one base pair is the 5′-end guanine and the complementary 3′-end cytosine. The relative energies of the deprotonated states compared with their radical cations are listed in Table 2. In this paper, the 5′-end guanine and 3′-end guanine are simply labeled as G_1 and G_2, and their complementary 3′-end cytosine and 5′-end cytosine are labeled as C_1 and C_2, respectively.

In Table 2, configurations in the second row are extracted from the optimized geometries **1** and **1d**, in which sodium ions are placed at low ESP positions. Configurations in the third row come from the optimized geometries **2** and **2d** with sodium ions at the high ESP positions. The stabilization energy differences in the second and third rows reveal that the deprotonated state changes with the configurations of the G−C pair. When the configuration of a single G−C pair is extracted from the geometries with sodium ions at low ESP positions, the stabilization energy decreases from 0.276 to −1.152 kcal/mol with inclusion of solvent effect. When one G−C pair is extracted from the geometries with sodium ions at high ESP positions, the stabilization energy without the PCM solvent environment is −1.504 kcal/mol, which is only 0.2 kcal/mol higher than the MP2 calculation.[23] The corresponding stabilization energy with

Table 2. Relative Energies of Deprotonated States Compared with Their Radical Cations [E(G(−H)·:C(+H)$^+$) − E(G·$^+$:C)]

relative energy (kcal/mol)	one G−C pair (G_1−C_1)	two G−C pairs	d[GG]
sodium ions placed at low	+0.276 [a]	+5.031	
ESP positions	(−1.152) [b]	(+1.802)	+1.92 [c]
sodium ions placed at high	−1.504	+5.160	
ESP positions	(−2.305)	(+0.776)	−0.71 [c]

[a] The energy differences are calculated at the B97D/6-31G(d) level. [b] Values in parentheses include PCM solvent. [c] The optimized results from ONIOM(Amber:B97D/6-31G(d)) + PCM method.

Table 3. NBO Charge Distributions (e) for Four Optimized d[GG] Oligomers

	1	1d	2	2d
G_1	0.4490	−0.0815	0.4711	−0.0715
C_1	0.0960	0.8108	0.0807	0.8065
G_2	0.3679	0.2030	0.3510	0.1879
C_2	0.0872	0.0676	0.0972	0.0771
intrabase proton	0.4556	0.4652	0.4559	0.4640

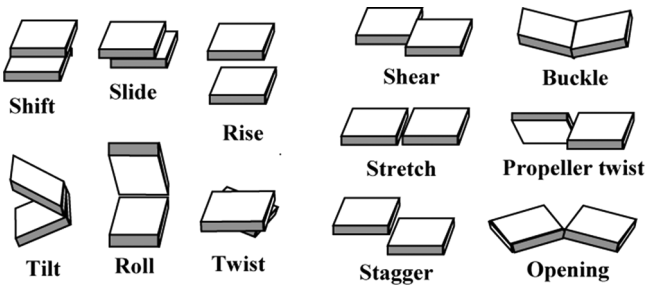

Figure 4. Local base-step parameters of two sequential bases and local base-pair parameters of a complementary base pair.

the solvent effect decreases by 0.8 kcal/mol. Therefore, the solvent effect helps the proton migrate from guanine to cytosine. Stabilization energies of two G−C pairs are all positive. That is to say, the interaction of π-stacking makes the deprotonation process unfavorable. The negative stabilization energy of d[GG] oligomer indicates that the sugar−phosphate backbone might contribute to the deprotonation process.

(C). Charge Distributions and Geometry Parameters. The NBO charge distributions of the four optimized d[GG] oligomers are listed in Table 3. Here, the charge distributions are analyzed within individual nucleobases. To reveal how the proton transfer affects the charge distribution, NBO charges on the intrabase proton are also listed. For oligomers **1** and **2** without proton transfer, 80% of the charge is delocalized on G_1 and G_2. This result is consistent with the previous ONIOM calculations.[14] For oligomers **1d** and **2d**, with a proton transferred from G_1 to C_1, the charge on C_1 increases to 0.81e, of which the transferred proton brings 0.46e charge from G_1 to C_1. As a result, the deprotonated state leaves about 0.73e charge localized on the first G−C pair. This value is close to the CPMD simulation on deprotonated Z-DNA oligomers,[12] in which the spin density localizes on one G−C pair and the value of its total spin angular momentum $\langle S^2 \rangle$ is 0.8. In summary, NBO analysis shows that the deprotonated state in a DNA oligomer leads to the localization of the positive charge on a single G−C base pair.

The geometry parameters of four optimized oligomers were calculated by the 3DNA package.[54] Six local *base-step* parameters (shift, slide, rise, tilt, roll and twist), shown in Figure 4, were used to identify the relation between two adjacent bases. The first three geometry parameters represent the translation of the second base with respect to the first base, and the last three parameters represent their torsion. Six local *base-pair* parameters (shear, stretch, stagger, buckle, propeller twist, and opening), which are also shown in Figure 4, are implemented to describe the geometry between complementary base pairs. Geometry parameters listed in Table 4 describe the relation between G_1 and G_2, and the relation between G_1 and C_1. **1** and **2d** are the stable oligomers corresponding to the two possible Na^+ arrangements. The local base-pair parameters of oligomers **1** and **2d** are very similar, which indicates it is the interaction between G_1 and C_1 that dominates the stabilization.

Table 4. Geometry Parameters of Optimized d[GG] Oligomers

		shift	slide	rise	tilt	roll	twist
G_1-G_2	**1**	−0.64	−1.24	3.25	−6.06	1.03	24.51
	1d	−1.24	−0.6	3.20	−3.63	−2.42	29.67
	2	−1.07	−0.75	3.30	−5.73	−3.55	44.98
	2d	−1.39	−0.55	3.26	−5.35	−3.08	35.67
		shear	stretch	stagger	buckle	propeller	opening
G_1-C_1	**1**	−0.16	−0.11	0.26	10.96	−10.86	1.03
	1d	−0.12	−0.19	0.23	7.14	−6.12	−4.56
	2	−0.06	−0.10	0.65	20.61	−6.34	−1.18
	2d	−0.13	−0.21	0.36	11.04	−11.94	−3.63

Table 5. Optimized Distances (Å) between X (X=N, O) and H in G_1-C_1 Base Pairs

	O_6-H	$H-N_4$	N_1-H	$H-N_3$	N_2-H	$H-O_2$
1	1.912[a]	1.029	1.057	1.799	1.045	1.695
	1.956[b]	1.019[b]	1.062[b]	1.761[b]	1.059[b]	1.608[b]
	2.174[c]	0.999[c]	1.022[c]	1.941[c]		1.768[c]
	2.005[d]			1.799[d]	1.018[c]	1.630[d]
2d	1.701[a]	1.052	1.716	1.077	1.027	1.837
	1.650[b]	1.050[b]	1.734[b]	1.069[b]	1.02[b]	1.904[b]
	1.777[d]		1.817[d]			1.913[d]

[a] Present work. [b] Ref 29. [c] Ref 30. [d] Ref 32.

Table 6. Optimized Hydrogen Bonds in G_1-C_1 Base Pairs[a]

	1	1d	2	2d
$d(O_6-H-N_4)$	2.941[b]	2.737	2.881	2.751
	2.97[c]			
$\angle(O_6-H-N_4)$	178.33[b]	176.62	173.00	175.35
	180.0[c]			178.0[c]
$d(N_1-H-N_3)$	2.856[b]	2.829	2.853	2.792
	2.82[c] (2.855[e])			2.869[d]
$\angle(N_1-H-N_3)$	177.73[b]	177.79	175.57	177.01
	173.1[c]			179.4[c]
$d(N_2-H-O_2)$	2.738[b]	2.906	2.800	2.863
	2.67[c]			
$\angle(N_2-H-O_2)$	176.29[b]	177.60	178.53	176.70
	178.6[c]			172.0[c]

[a] Distances, in angstroms; angles, in degrees. [b] Present work. [c] Ref 29. [d] Ref 30. [e] Ref 32.

There are three hydrogen bonds between G_1 and C_1: $O_6(G_1)\cdots H-N_4(C_1)$, $N-H\cdots N$, and $N_2(G_1)-H\cdots O_2(C_1)$. The hydrogen bond $N-H\cdots N$ changes its form from $N_1(G_1)-H\cdots N_3(C_1)$ to $N_1(G_1)\cdots H-N_3(C_1)$ within the deprotonation process in the G_1-C_1 pair. The optimized distances between X (X=O, N) and H for oligomers **1** and **2d** are listed in Table 5. These results are very close to the previous

Table 7. The Stabilization Energies $E(2)$ of Hydrogen Bonds in G_1-C_1 Base Pairs Based on Second-Order Perturbation NBO Analysis[a]

$E(2)$ (kcal/mol)	1	1d	2	2d
$n(N(G_1 \text{ or } C_1)) \rightarrow \sigma^*(H-N(C_1 \text{ or } G_1))$	14.30	17.85	14.11	20.17
$n(O_6(G_1)) \rightarrow \sigma^*(H-N_4(C_1))$	5.28 (2.54)	14.06 (3.81)	6.18 (2.93)	13.20 (3.70)
$n(O_2(C_1)) \rightarrow \sigma^*(H-N_2(G_1))$	10.96 (4.31)	4.74 (2.96)	8.54 (3.66)	5.29 (3.46)

[a] Values in parentheses are the stabilization energies between the second lone pair of the oxygen and the antibonding $\sigma^*(N-H)$.

B3LYP/6-31G** calculations;[29] therefore, the two groups of data are well matched. The R^2 value of linear fitting is 0.988. The largest differences are the distances of $H\cdots O_2(C_1)$: 0.087 Å for oligomer **1** and 0.067 Å for oligomer **2d**.

For the above three kinds of hydrogen bonds $X-H\cdots Y$ (X, Y = O, N), distances between X and Y and bond angles of $\angle X-H\cdots Y$ are listed in Table 6. It can be observed that the distance between $N_1(G_1)$ and $N_3(C_1)$ decreases by 0.064 Å when the deprotonation process happens. Meanwhile, the distance between $O_6(G_1)$ and $N_4(C_1)$ significantly decreases by 0.190 Å, and the distance between $N_2(G_1)$ and $O_2(C_1)$ increases by 0.125 Å. These distance distortions come from a corresponding distance decrease in $O_6(G_1)\cdots H$ and distance increase in $H\cdots O_2(C_1)$. The simultaneous distortions of these three hydrogen bonds have been theoretically investigated by DFT calculations,[57] and a small polaron has been defined to describe this distortion.

(D). Natural Bond Orbital Analysis. Second-order perturbation estimates of donor−acceptor interactions based on natural bond orbitals (NBOs) were employed to study the intermolecular orbital interactions in the G_1-C_1 pair. In this estimate, the donors are Lewis-type NBOs, and the acceptors are antibonding NBOs. Interaction between donors and acceptors leads to donation of charge from the occupied NBOs into the empty NBOs. The corresponding second-order energy, $E(2)$, represents the stabilization energy of charge delocalization from each NBO donor to NBO acceptor. This second-order perturbation NBO analysis can be applied to investigate the stabilization of a hydrogen bond $X-H\cdots Y$.[58,59] Here, the NBO donor is the lone pair orbital of atom Y, which is labeled as $n(Y)$. The NBO acceptor is the antibonding orbital σ^* of the X−H bond, which is labeled as $\sigma^*(X-H)$.

Second-order perturbation NBO analyses were performed on two G−C base pairs, which were extracted from four optimized oligomers. The five largest $E(2)$ values between G_1-C_1 pairs are listed in Table 7. The most stable hydrogen bond is the $N-H\cdots N$. The stabilization energies of the hydrogen bond $N_1(G_1)-H\cdots N_3(C_1)$ are 14.30 and 14.11 kcal/mol for **1** and **2**, respectively. The stabilization energies of hydrogen bond $N_1(G_1)\cdots H-N_3(C_1)$ are 17.85 and 20.17 kcal/mol for **1d** and **2d**, respectively. It is obvious that the $N_1(G_1)\cdots H-N_3(C_1)$ bond in **2d** is very stable. The $O\cdots H-N$ bonds are also stable hydrogen bonds. The $E(2)$ values in parentheses in Table 7 are the stabilization energies between the second lone pair of oxygen and the antibonding $\sigma^*(N-H)$. When the deprotonation process happens, the changes of $E(2)$ values for $O\cdots H-N$ are not as significant as the change for the $N_1(G_1)\cdots H-N_3(C_1)$ bond in **2d**. That is to say, it is the extreme stabilization of the $N_1(G_1)\cdots H-N_3(C_1)$ bond that causes oligomer **2d** to be more stable than oligomer **2**.

In summary, the $N-H\cdots N$ hydrogen bond in the guanine−cytosine pair provides an important contribution to the stabilization of poly(G)−poly(C) oligomers. For some deprotonated configurations induced by different counterion arrangements, the $N_1(G_1)\cdots H-N_3(C_1)$ bond provides an extreme stabilization to the proton transfer state.

IV. CONCLUSIONS

The ONIOM + PCM method was employed to investigate the process of proton transfer in a guanine−cytosine pair of the B-form d[GG] radical cation. Using the ONIOM method, high-level DFT calculations were applied to all complementary base pairs. The B97D functional, which describes the dispersion interaction between π-stacked nucleobases, was adopted to perform these calculations. The entire ONIOM system, including the sugar−phosphate backbone and counterions, was described by the AMBER99SB/parmbsc0 force field. The solvent effect was included using the polarizable continuum model. This ONIOM + PCM optimization provides reasonable geometries of DNA oligomers.

The stabilization of the deprotonated state in d[GG] oligomer is related to the arrangement of sodium ions. When sodium ions are located near phosphate groups, the proton prefers bonding with the guanine, and 80% of the charge is delocalized on the guanine residues. When sodium ions are placed in the major groove, the deprotonated state is favored. Combining with the proton transfer, 70% of the charge localizes on the corresponding guanine−cytosine pair. In conclusion, the arrangement of counterions is very important in the optimization of DNA configurations, especially for the study of the proton transfer process in a guanine−cytosine pair of poly(G)−poly(C) radical cation.

Natural bond orbital analysis was performed on the optimized geometries. The results show that the $N-H\cdots N$ hydrogen bond in the guanine−cytosine pair provides an important contribution to the stabilization of the deprotonated state. The stabilization of this hydrogen bond is very sensitive to the d[GG] oligomer configuration.

AUTHOR INFORMATION

Corresponding Author

*Phone: (902)494-8883. Fax: (902)494-1310. E-mail: Russell.Boyd@dal.ca.

ACKNOWLEDGMENT

The financial support of the Natural Sciences and Engineering Research Council (NSERC) of Canada is gratefully appreciated. The use of computing resources provided by WestGrid and Compute/Calcul Canada is graciously acknowledged. Computational facilities were also provided by ACEnet, the regional high performance computing consortium for universities in Atlantic Canada. ACEnet is funded by the Canada Foundation for Innovation (CFI), the Atlantic Canada Opportunities Agency (ACOA), and the provinces of Newfoundland and Labrador, Nova Scotia, and New Brunswick.

REFERENCES

(1) Núñez, M. E.; Hall, D. B.; Barton, J. K. *Chem. Biol.* **1999**, *6*, 85–97.
(2) Meggers, E.; Michel-Beyerle, M. E.; Giese, B. *J. Am. Chem. Soc.* **1998**, *120*, 12950–12955.
(3) Liu, C-S; Schuster, G. B. *J. Am. Chem. Soc.* **2003**, *125*, 6098–6102.
(4) Steenken, S.; Jovanovic, S. V. *J. Am. Chem. Soc.* **1997**, *119*, 617–618.
(5) Wetmore, S. D.; Boyd, R. J.; Eriksson, L. A. *Chem. Phys. Lett.* **2000**, *322*, 129.
(6) Senthilkumar, K.; Grozema, F. C.; Guerra, C. F.; Bickelhaupt, F. M.; Lewis, F. D.; Berlin, Y. A.; Ratner, M. A.; Siebbeles, L. D. A. *J. Am. Chem. Soc.* **2005**, *127*, 14894–14903.
(7) *Top. Curr. Chem.*; Schuster, G. B., Ed.; Springer: Heidelberg, 2004; Vol. 236−237.
(8) *Charge Transfer in DNA*; Wagenknecht, H.-A., Ed.; Wiley-VCH: Weinheim, Germany, 2005.
(9) Shao, F.; O'Neill, M. A.; Barton, J. K. *Proc. Natl. Acad. Sci. U.S.A.* **2004**, *101*, 17914.
(10) Henderson, P. T.; Jones, D.; Hampikian, G.; Kan, Y. Z.; Schuster, G. B. *Proc. Natl. Acad. Sci. U.S.A.* **1999**, *96*, 835.
(11) Barnett, N. R.; Cleveland, C. L.; Joy, A.; Landman, U.; Schuster, G. B. *Science* **2001**, *294*, 567.
(12) Gervasio, F. L.; Laio, A.; Parrinello, M.; Boero, M. *Phys. Rev. Lett.* **2005**, *94*, 158103.
(13) Mallajosyula, S. S.; Gupta, A.; Pati, S. K. *J. Phys. Chem. A* **2009**, *113*, 3955.
(14) (a) Wu, J.; Walker, V. J.; Boyd, R. J. *J. Phys Chem. B* **2011**, *115*, 3136. (b) Wu, J.; Walker, V. J.; Boyd, R. J. *J. Phys Chem. B* **2011**, *115*, 8949.
(15) Conwell, E. M.; Bloch, S. M. *J. Phys. Chem. B* **2006**, *110*, 5801.
(16) Kalosakas, G.; Rasmussen, K. Ø.; Bishop, A. R. *J. Chem. Phys.* **2003**, *118*, 3731.
(17) Wei, J. H.; Wang, L. X.; Chan, K. S.; Yan, Y. J. *Phys. Rev. B* **2005**, *72*, 064304.
(18) Singh, M. R. *Phys. Stat. Sol. C* **2005**, *2*, 2970.
(19) Zhang, G. Q.; Cui, P.; Wu, J.; Liu, C. B. *Chem. Phys. Lett.* **2009**, *471*, 163.
(20) Grozema, F. C.; Siebbeles, L. D. A.; Berlin, Yu. A.; Ratner, M. A. *Chem. Phys. Chem.* **2002**, *3*, 536.
(21) Kurnikov, I. V.; Tong, G. S. M.; Madrid, M.; Beratan, D. N. *J. Phys. Chem. B* **2002**, *106*, 7.
(22) Voityuk, A. A. *J. Chem. Phys.* **2005**, *122*, 204904.
(23) Kubař, T.; Elstner, M. *J. Phys. Chem. B* **2008**, *112*, 8788.
(24) Kumar, A.; Sevilla, M. D. *J. Phys. Chem. B* **2011**, *115*, 4990.
(25) (a) Steenken, S. *Biol. Chem.* **1997**, *378*, 1293. (b) Steenken, S. *Chem. Rev.* **1989**, *89*, 503–520.
(26) Giese, B. *Top. Curr. Chem.* **2004**, *236*, 27–44.
(27) Kawai, K.; Osakada, Y.; Majima, T. *Chem. Phys. Chem.* **2009**, *10*, 1766.
(28) Adhikary, A.; Khanduri, D.; Sevilla, M. D. *J. Am. Chem. Soc.* **2009**, *131*, 8614.
(29) Bertran, J.; Oliva, A.; Rodriguez-Santiego, L.; Sodupe, M. *J. Am. Chem. Soc.* **1998**, *120*, 8159.
(30) Hutter, M.; Clark, T. *J. Am. Chem. Soc.* **1996**, *118*, 7574.
(31) Li, X. F.; Sevilla, M. D. *Adv. Quantum Chem.* **2007**, *52*, 59.
(32) Kumar, A.; Sevilla, M. D. *J. Phys Chem. B* **2009**, *113*, 11359.
(33) Cerón-Carrasco, J. P.; Requena, A.; Perpète, E. A.; Michaux, C.; Jacquemin, D. *J. Phys Chem. B* **2010**, *114*, 13439.
(34) Voityuk, A. A.; Siriwong, K.; Rösch, N. *Phys. Chem. Chem. Phys.* **2001**, *3*, 5421.
(35) Olofsson, J.; Larsson, S. *J. Phys. Chem. B* **2001**, *105*, 10398.
(36) Troisi, A.; Orlandi, G. *J. Phys. Chem. B* **2002**, *106*, 2093.
(37) Voityuk, A. A. *J. Phys. Chem. B* **2005**, *109*, 10793.
(38) Conwell, E. M.; Bloch, S. M.; McLaughlin, P. M.; Basko, D. M. *J. Am. Chem. Soc.* **2007**, *129*, 9175.
(39) Mantz, Y. A.; Gervasio, F. L.; Laino, T.; Parrinello, M. *Phys. Rev. Lett.* **2007**, *99*, 058104.
(40) Shapir, E.; Cohen, H.; Calzolari, A.; Cavazzoni, C.; Ryndyk, D. A.; Cuniberti, G.; Kotlyar, A.; Felice, R. D.; Porath, D. *Nat. Mater.* **2008**, *7*, 68.
(41) Dapprich, S.; Komáromi, I.; Byun, K. S.; Morokuma, K.; Frisch, M. J. *J. Mol. Struct. (Theochem)* **1999**, *462*, 1.
(42) Vreven, T.; Morokuma, K.; Farkas, Ö.; Schlegel, H. B.; Frisch, M. J. *J. Comput. Chem.* **2003**, *24*, 760.
(43) Macke, T.; Case, D. A. Modeling unusual nucleic acid structures. In *Molecular Modeling of Nucleic Acids*, Leontes, N. B., SantaLucia, J., Jr., Eds.; American Chemical Society: Washington, D.C: 1998, pp 379−393.
(44) Case, D. A.; Cheatham, T. E., III; Darden, T.; Gohlke, H.; Luo, R.; Merz, K. M.; Onufriev, A., Jr.; Simmerling, C.; Wang, B.; Woods., R. *J. Computat. Chem.* **2005**, *26*, 1668.
(45) Liu, T.; Barton, J. K. *J. Am. Chem. Soc.* **2005**, *127*, 10160.
(46) Grimme, S. *J. Comput. Chem.* **2006**, *27*, 1787.
(47) Ducéré, J.-M.; Cavallo, L. *J. Phys. Chem. B* **2007**, *111*, 13124.
(48) Peverati, R.; Baldridge, K. K. *J. Chem. Theory Comput.* **2008**, *4*, 2030.
(49) Kolář, M.; Kobař, T.; Hobza, P. *J. Phys. Chem. B* **2011**, *115*, 8038.
(50) Wang, J.; Cieplak, P.; Kollman, P. A. *J. Comput. Chem.* **2000**, *21*, 1049.
(51) Best, R. B.; Buchete, N.-V.; Hummer, G. *Biophys. J.* **2008**, *95*, 4494.
(52) Perez, A.; Marchan, I.; Svozil, D.; Šponer, J.; Cheatham, T. E.; Laughton, C. A.; Orozco, M. *Biophys. J.* **2007**, *92*, 3817.
(53) Vreven, T.; Mennucci, B.; da Silva, C. O.; Morokuma, K.; Tomasi, J. *J. Chem. Phys.* **2001**, *115*, 62.
(54) Weinhold, F. Natural Bond Orbital Methods. In *Encyclopedia of Computational Chemistry*, Schleyer, P. v. R.; Allinger, N. L.; Clark, T.; Gasteiger, J.; Kollman, P. A.; Schaefer, H. F., III; Schreiner, P. R., Eds.; John Wiley & Sons: Chichester, UK, 1998, Vol. 3, pp 1792−1811.
(55) Frisch, M. J.; Trucks, G. W.; Schlegel, H. B.; Scuseria, G. E.; Robb, M. A.; Cheeseman, J. R.; Scalmani, G.; Barone, V.; Mennucci, B.; Petersson, G. A.; Nakatsuji, H.; Caricato, M.; Li, X.; Hratchian, H. P.; Izmaylov, A. F.; Bloino, J.; Zheng, G.; Sonnenberg, J. L.; Hada, M.; Ehara, M.; Toyota, K.; Fukuda, R.; Hasegawa, J.; Ishida, M.; Nakajima, T.; Honda, Y.; Kitao, O.; Nakai, H.; Vreven, T.; Montgomery, J. A., Jr.; Peralta, J. E.; Ogliaro, F.; Bearpark, M.; Heyd, J. J.; Brothers, E.; Kudin, K. N.; Staroverov, V. N.; Kobayashi, R.; Normand, J.; Raghavachari, K.; Rendell, A.; Burant, J. C.; Iyengar, S. S.; Tomasi, J.; Cossi, M.; Rega, N.; Millam, N. J.; Klene, M.; Knox, J. E.; Cross, J. B.; Bakken, V.; Adamo, C.; Jaramillo, J.; Gomperts, R.; Stratmann, R. E.; Yazyev, O.; Austin, A. J.; Cammi, R.; Pomelli, C.; Ochterski, J. W.; Martin, R. L.; Morokuma, K.; Zakrzewski, V. G.; Voth, G. A.; Salvador, P.; Dannenberg, J. J.; Dapprich, S.; Daniels, A. D.; Farkas, Ö.; Foresman, J. B.; Ortiz, J. V.; Cioslowski, J.; Fox, D. J. *Gaussian09*; Gaussian, Inc.: Wallingford, CT, 2009.
(56) Humphrey, W.; Dalke, A.; Schulten, K. *J. Mol. Graphics* **1996**, *14*, 33.
(57) Alexandre, S. S.; Artacho, E.; Soler, J. M.; Chacham, H. *Phys. Rev. Lett.* **2003**, *91*, 108105.
(58) Sosa, G. L.; Peruchena, N. M.; Contreras, R. H.; Castro, E. A. *J. Mol. Struct. Theochem.* **2002**, *577*, 219.
(59) Yuan, X.-X.; Wang, Y.-F.; Wang, X.; Chen, W.; Fossey, J. S.; Wong, N.-B. *Chem. Cent. J.* **2010**, *4*, 6.